Published in final edited form as:
Acta Neuropathol. 2013 May ; 125(5): 727–739. doi:10.1007/s00401-013-1103-z.

Epigenetic regulation of cholinergic receptor M1 (CHRM1) by histone H3K9me3 impairs Ca2+ signaling in Huntington's disease

Junghee Lee[1,2,#], **Yu Jin Hwang**[3,#], **Jong-Yeon Shin**[4,6,#], **Won-Chul Lee**[3,4,#], **Jinhong Wie**[5,#], **Ki Yoon Kim**[3], **Min Young Lee**[7], **Daehee Hwang**[7], **Rajiv R. Ratan**[8], **Ae Nim Pae**[9], **Neil W. Kowall**[1,2], **Insuk So**[5], **Jong-Il Kim**[4,6], and **Hoon Ryu**[1,2,3,*]

[1]Veteran's Affairs Boston Healthcare System, Boston, MA 02130, USA

[2]Department of Neurology and Boston University Alzheimer's Disease Center, Boston University School of Medicine, Boston, MA 02118, USA

[3]WCU Neurocytomics Group, Seoul National University College of Medicine, Seoul, South Korea

[4]Genome Medicine Institute, Seoul National University College of Medicine, Seoul, South Korea

[5]Department of Physiology and Biomedical Sciences, Seoul National University College of Medicine, Seoul, South Korea

[6]Psoma Therapeutics Inc. Seoul, South Korea

[7]School of Interdisciplinary Bioscience and Bioengineering and Department of Chemical Engineering, POSTECH, Pohang, South Korea

[8]Burke Medical Research Institute, White Plains, NY, USA

[9]Center for Neuro-Medicine, Brain Science Institute, Korea Institute of Science and Technology (KIST), Hwarangno 14-gil 5, Seongbuk-gu, Seoul 136-791, South Korea

Abstract

Huntington's disease (HD) is an autosomal dominant neurodegenerative disease caused by an expanded trinucleotide CAG repeat in the gene coding for huntingtin (Htt). Deregulation of chromatin remodeling is linked to the pathogenesis of HD but the mechanism remains elusive. In order to identify what genes are deregulated by trimethylated histone H3K9 (H3K9me3)-dependent heterochromatin, we performed H3K9me3-ChIP genome-wide sequencing combined with RNA-sequencing followed by platform integration analysis in stable striatal HD cell lines (ST*Hdh*Q7/7 and ST*Hdh*Q111/111 cells). We found that genes involving neuronal synaptic transmission including cholinergic receptor M1 (CHRM1), cell motility, and neuronal differentiation pathways are down regulated while their promoter regions are highly occupied with H3K9me3 in HD. Moreover, we found that repression of *CHRM1* gene expression by H3K9me3 impairs Ca^{2+}-dependent neuronal signal transduction in stable cell lines expressing mutant HD protein. Thus, our data indicates that the epigenetic modifications, such as aberrant H3K9me3-dependent heterochromatin plasticity, directly contribute to the pathogenesis of HD.

[*]To whom correspondence should be addressed: Hoon Ryu, Ph.D., Department of Neurology, Boston University School of Medicine, VA Boston Healthcare System, Building 1A, Rm109, 150 South Huntington Avenue, Boston, MA 02130 USA, Tel: 857-364-5910, Fax: 857-364-4540, hoonryu@bu.edu.
[#]These authors are equally contributed.

Keywords

H3K9me3; epigenomes; Huntington's disease; cholinergic receptor M1; heterochromatin

Introduction

Huntington's disease (HD), an incurable and fatal autosomal dominant disorder of mid-life onset characterized by chorea and progressive cognitive decline, is caused by an expansion of CAG repeats coding for glutamine (Q) in exon 1 of the *Huntingtin* (*Htt*) gene [24]. Alterations of chromatin structure and deregulation of neuronal gene transcription are prominent features of HD. Chromatin remodeling through histone acetylation and methylation in the N-terminal lysine residues modulates the transcription of nuclear genes [7, 8, 35] As such, altered nucleosome dynamics via histone modifications may result in transcriptional dysfunction [6, 18]. Indeed, transcriptional anomalies are observed in HD, where a subset of genes identified in expression profiling studies is markedly deregulated. Reduced gene transcription in HD has recently been associated with alterations in histone acetylation and methylation profiles [6, 18, 19, 22]. Altered transcriptional activity is thought to be an important factor leading to neuronal death in HD.

We previously found that abnormal induction of histone methyltransferase (HMT) expression and increased trimethylated histone H3K9 (H3K9me3) is correlated with transcriptional dysfunction and neurodegeneration in animal models of HD and in HD patients [6, 18, 22]. Histone H3K9me3 code is associated with decreased transcriptional activity and heterochromatin condensation while H3K9 acetylation improves transcription [8, 30, 31]. To date, however, the mechanisms of H3K9me3-dependent neuronal gene silencing and the transcriptome specifically targeted by H3K9me3 have not been fully investigated in HD [18, 20, 26, 34]. Therefore, a major question is whether the heterochromatin remodeling driven by H3K9me3 is directly linked to the pathogenesis of HD and, if so, how does the targeted genome and transcriptome modulated by H3K9me3 contribute to a neuronal dysfunction in HD.

To determine what genes are occupied by nucleosomes containing H3K9me3 in HD, we used H3K9me3-chromatin immunoprecipitation (ChIP) with massively parallel DNA sequencing (ChIP-Seq) and RNA transcriptome-sequencing followed by platform integration analysis [15, 36]. While the occupancy of H3K9me3 is increased in the promoter region, the level of mRNAs is inversely down regulated in subsets of key genomes encoding neuronal synaptic transmission, differentiation, and cell motility in HD. We further verified that repression of the CHRM1 gene is directly linked to impaired Ca^{2+}-dependent neuronal transmission in response to acetylcholine in HD. These data indicate that epigenetic mechanisms driven by the aberrant heterochromatin remodeling via hypertrimethylation of H3K9 are important factors contributing to neuronal death in HD.

Materials and methods

Cell Culture and Transfection Assays

ST*Hdh*Q7/7 (wild type) and ST*Hdh*Q111/111 (HD knock-in striatal cell line expresses mutant huntingtin at endogenous level), were generously provided from Dr. Marcy MacDonald (Harvard Medical School) [25]. For transfection assays, 2.5×10^5 cells were plated onto 48-well cell culture plates 24 h prior to transfection. DMRIE-C reagent (Invitrogen) has been used as a transfection reagent and transfections were performed according to the manufacturer's protocol.

Animals

Male R6/2 mice were bred with females from their background strain (B6CBAFI/J), and offspring were genotyped using PCR [18, 33]. CAG repeat length remained stable within a 147–153 range. Female mice were used in the experimental paradigms.

Confocal Microscopy

Cells were immunostained for trimethylated histone H3K9 (H3K9me3) (rabbit antibody; dilution, 1:200; Upstate Biotech.) and ESET/SETDB1 (ESET antibody; dilution, 1:200; Upstate Biotech.) using a previously reported conjugated second antibody method [17]. For the immunocytochemistry, antibody complexes were visualized using diaminobenzidine. For the confocal microscopy, the specimens were incubated for 1 h with fluorescence (FITC)-conjugated goat anti-mouse IgG antibody (Vector, Burlingame, CA) and Cy3-conjugated anti-rabbit IgG antibody (Jackson Lab.) after the incubation of primary antibody. Images were analyzed using a Spinning Disk Confocal microscope (IX2-DSU, Olympus). Preabsorbtion with excess target protein or omission of primary antibody was used to demonstrate antibody specificity and background generated from the detection assay.

Chromatin Immunoprecipitation (ChIP)-qPCR assay

ChIP for H3K9me3 binding to DNA was performed using a CHIP assay kit (Santa Cruz) as described previously [17]. ST*Hdh*Q7/Q7 and ST*Hdh*Q111/Q111 cells were crossed-linked with 1% formaldehyde for 20 min at room temperature. The lysates were sonicated six times with each time for 30 sec using Bioruptor (Diagenode Inc., NJ, USA). After centrifugation, the supernatant was diluted in CHIP dilution buffer and then incubated overnight at 4 °C with anti-H3K9me3 antibody. Immune complexes were recovered by the addition of 60 μl of salmon sperm DNA/protein A agarose-50% slurry and incubation for 2hr at 4 °C with rotation. The beads were pelleted and washed with low and high salt buffer and finally three times with LiCl buffer. The immune complexes were eluted by incubation for 4 hr at 66 °C with 500 μl of fresh elution buffer (1% SDS, 0.1M $NaHCO_3$) and 20 μl of 5M NaCl. The DNA cleaned by the addition of 2 μl of 500mM EDTA, μl of 1M Tris and 1 μl of proteinase K. The DNA solution is extracted with a phenol/chloroform/isoamyl alcohol mixture to remove protein contaminants, then precipitated with 100% ethanol. After the precipitation step, the pellet washed with 70% ethanol and dissolved in 20 μl DW. The sequences of ChIP validation primers are shown in the Supplementary Information.

Quantitative Real Time-PCR (qRT-PCR)

Fifty nanograms of RNA were used as a template for qRT-PCR amplification, using SYBR Green Real-time PCR Master Mix (Toyobo, Japan). Two-step PCR thermal cycling for DNA amplification and real-time data acquisition were performed with an ABI StepOnePlus™ Real-Time PCR System using the following cycle conditions: 95°C for 1min × 1 cycle, and 95°C for 15s, followed by 60°C for 1min × 40cycles. Fluorescence data were analyzed by the ABI StepOnePlus software and expressed as C_T, the number of cycles needed to generate a fluorescent signal above a predefined threshold. The ABI StepOnePlus software set baseline and threshold values. Primers were standardized in the linear range of cycles prior to onset of the plateau. The mRNA was normalized to GAPDH. The sequences of mRNA validation primers are shown in the Supplementary Table 4.

ChIP-sequencing and gene analysis

ChIP DNA samples were then subjected to preparation for ChIP-Seq Library construction: the libraries were constructed following Illumina's Chip-Seq Sample prep kit. Briefly, Chip DNA was end-blunted and added with an 'A' base so the adaptors from Illumina with a 'T' can ligate on the ends. Then 200–400 bp fragments are gel-isolated and purified. The library

was amplified by 18 cycles of PCR. The resulting DNA libraries were quantified by an Agilent DNA 1000 series II assay and a Nanodrop 7500 spectrophotometer using a 1.5 μl aliquot that was diluted to 10 nM. We performed cluster generation and 36 cycles of sequencing on the Illumina cluster station and Genome Analyzer IIx following the manufacturer's instructions. The sequencing facility (Genome Medicine Institute, Korea) has generated libraries for three biological replicates. Primary analysis of ChIP-Seq data sets: the image analysis and base calling were performed by using Illumina's Genome Analysis pipeline. The sequencing reads were aligned to the mouse genome UCSC build mm9 by using GSNAP alignment programs [32]. Only uniquely aligned reads were kept for downstream analysis. The read mapping on the genome, algorism, and conversion of RPKM were performed as previously described [15]. Gene ontology analysis: the gene ontology analysis was carried out by using DAVID/EASE [9].

Whole transcriptome sequencing (RNA-seq) and gene analysis

For the mRNA-Seq sample preparation, the Illumina standard kit was used according to the manufacturer's protocol. Briefly, 3 μg of each total RNA sample was used for polyA mRNA selection using streptavidin-coated magnetic beads, followed by thermal mRNA fragmentation. The fragmented mRNA was subjected to cDNA synthesis using reverse transcriptase (SuperScript II) and random primers. The cDNA was further converted into double stranded cDNA and, after an end repair process (Klenow fragment, T4 polynucleotide kinase and T4 polymerase), was finally ligated to Illumina paired end (PE) adaptors. Size selection was performed using a 2% agarose gel, generating cDNA libraries ranging in size from 200–250 bp. Finally, the libraries were enriched using 10 cycles of PCR and purified by the QIAquick PCR purification kit (Qiagen). The enriched libraries were diluted with Elution Buffer to a final concentration of 10 nM. Each library was run at a concentration of 8 pM on one Genome Analyzer (GAIIx) lane using 53 bp sequencing. Reads were then processed and aligned to the mouse genome UCSC build mm9 using GSNAP [32]. GSNAP uses the normalized RNA-Seq fragment counts to measure the relative abundances of transcripts. The unit of measurement is Reads Per Kilobase of exon per Million fragments mapped (RPKM) [15].

H3K9me3 gene structural occupancy

The H3K9me3 occupancies for 4 different gene structures (5kb upstream, 5′ UTR, CDS, and 3′ UTR) were binned by 100 and the coverage of each bin was estimated by averaging all genes' values. When calculating the occupancies of 5′ UTR, CDS, and 3′ UTR, only the genes whose corresponding gene structure size is bigger than 1,000 were considered.

Functional enrichment analysis and network analysis

We performed enrichment analysis of GO biological processes (GOBPs) for genes in which both H3K9me3 and mRNA levels are deregulated in HD using DAVID [9]. (Supplementary Table 1, 2). A number of cellular processes were significantly represented by the 545 genes with increased H3K9me3 and decreased mRNA levels (Supplementary Table 1). For network analysis among the 545 genes, we focused on 56 genes involved in three groups of processes: 1) synaptic transmission, 2) axon guidance, and 3) cytoskeleton organization (Supplementary Table 1). We then generated a network model to delineate the relationships of the 56 genes and their associated processes. For each of the above three groups of processes, we first generated subnetworks for the genes, called seeds, belonging to the processes using MetaCore™ (version 6.7) [4]- 'Analyze Networks' (AN) algorithm with the default option. Among the subnetworks resulting from the AN algorithm, we chose the top two ones and then combined them into a single subnetwork. This procedure was performed for all the three groups of processes, resulting in the three combined subnetworks, which were then merged to the final network. For the final network, to clarify the relationships of

the processes, we computed degree centrality (K) and shortest path centrality (SP) using CentiBiN [9, 11] and then pruned non-seed nodes with SP=0 or K=1. The network was visualized using Cytoscape (v. 2.7.0) [21]. The nodes with similar GOBPs or in the same KEGG pathways were grouped into the same modules, each of which was named by the corresponding GOBPs or KEGG pathway.

Ca^{2+} imaging

Cells were loaded in 5μM Fura 2-AM (Molecular Probes, Eugene, OR) and 0.01% pluronic acid in NT solution for 45 min at 33°C, and then unloaded in NT solution for another 15 min. The composition of the NT solution was constituted with NaCl, 145 mM; KCl, 3.6 mM; $MgCl_2$, 1 mM; $CaCl_2$, 1.3 mM; glucose, 5 mM; and HEPES (pH 7.4),10 mM. 24well plate with Fura 2-AM loaded cells was then transferred to a perfusion chamber on the stage of an upright microscope (Nikon ECLIPSE Ti LAMBDA DG-4). Cells were illuminated by a Xenon lamp and observed with a 40× UV water-immersion objective lens (NA: 0.8, LUMPlan FL 40W; Olympus, Tokyo, Japan). For Fura 2-AM excitation, the shutter and filter wheel (polychrome-IV; TILL-Photonics, Martinsried, Germany) were controlled by Axon Imaging Workbench (AIW) software 2.1 (Axon Instruments, Foster City, CA) to provide sequential illumination at two alternating wavelengths, 340 and 380 nm. Fluorescence of Fura 2-AM was detected at an emission wavelength of 510 nm. Video images were acquired using an intensified CCD camera (Sensicam, PCO, Kelheim, Germany). Fluorescence emission ratios following excitation at 340 and 380 nm were calculated by dividing averaged pixel values in circumscribed regions of individual responding cells in the field of view. The values were exported from AIW to Origin 8.0 for additional analysis and plotting. Two inhibitors, pirenzepine (100 μM) and methoctramine (10 μM), were used to determine whether the Ca^{2+} response is occurred via CHRM1-dependent pathway in striatal cells.

Western blot analysis

Western blot was performed as previously described [18]. Thirty μg of protein was subjected to SDS-PAGE (10%) and blotted with anti-H3K9me3 (Upstate Biotech.), anti-ESET and anti-CHRM1 (SantaCruz Biotech.) antibody. Protein loading was controlled by probing for alpha-tubulin (Sigma) on the same membrane.

Human tissue samples

Samples of striatum and the superior frontal cortex were pathologically verified and graded according to neuropathological criteria as described previously [18]. The information on human brain samples was shown in Supplementary Table 3.

Statistics

Data were analyzed using SigmaPlot. Paired, two-tailed t-tests were used as appropriate. Nonparametric tests were used for further analysis; unpaired t-tests and one-way ANOVAs were followed by Mann-Whitney and Kruskal-Wallis tests, respectively.

Results

Expansion of trimethylated histone H3K9 (H3K9me3)-dependent heterochromatin condensation in HD

The analysis of the spatiotemporal pattern of histone modifications such as heterochromatin condensation provides us relevant understanding of chromatin plasticity under neurodegenerative condition of HD [12, 18, 19]. In particular, trimethylation of H3K9 has been correlated with gene silencing and condensation of constitutive heterochromatin [12].

The complexity that can be achieved with this single modification in H3K9 is remarkable. Accordingly, in the first series of experiments, we determined H3K9me3 levels and changes in the volume of H3K9me3-dependent pericentromeric heterochromatin in HD cell lines (ST*Hdh*Q7/7 and ST*Hdh*Q111/111 cells). We examined the spatial distribution of pericentromeric heterochromatin and H3K9me3 in striatal neurons using confocal microscopy with 3-D reconstruction and image analysis (AQI-X-COMBO-CWF, Media cybernetics Inc. Bethesda, MD). The majority of H3K9me3 was localized to prominent clusters of pericentromeric heterochromatin (chromocenters) in mouse cells, whereas mono- and dimethylation states could not be resolved [22]. H3K9me3 immunoreactivity (red color) was distributed in small foci that colocalized with chromocenters (blue color stained with DAPI) in ST*Hdh*Q7/7 and ST*Hdh*Q111/111 cells (Fig. 1a). There was a robust increase in H3K9me3 immunoreactivity in ST*Hdh*Q111/111 cells compared to ST*Hdh*Q7/7 controls (Fig. 1a). Deconvolved images and image analysis data showed a two-fold increase in condensed H3K9me3-positive heterochromatin and an expansion of chromocenters in ST*Hdh*Q111/111 cells compared to ST*Hdh*Q7/7 controls (Fig. 1b, c). In addition, the surface area of H3K9me3-positive heterochromatin was elevated in ST*Hdh*Q111/111 cells (Fig. 1c). Levels of H3K9me3 protein determined by Western blot analysis were significantly increased in ST*Hdh*Q111/111 cells compared to ST*Hdh*Q7/7 cells consistent with immunocytochemical staining for H3K9me3 (Fig. 1d).

H3K9me3 ChIP sequencing, RNA sequencing, and integration analysis

Because H3K9me3 affects promoter landscaping and neuronal gene expression, we performed H3K9me3-ChIP genome-wide sequencing combined with RNA (transcriptome) sequencing (Fig. 2a and Fig. S1a, b). H3K9me3 occupancy was analyzed for six different genomic structures: intergenic, intronic, upstream, downstream, UTR, and CDS including chromosomes (Fig. 2a and Fig. S2). Upstream and downstream were defined as the 2kb genomic area away from the transcription start site and end site respectively (Fig. S2a). As sequencing reads represent only the ends of the ChIP fragments, we utilized a peak-finding algorithm, MACS, to extract H3K9me3-occupied genomic positions [36]. We ran MACS with default parameters and obtained 164,324 and 82,276 peaks for ST*Hdh*Q7/7 and ST*Hdh*Q111/111 cells respectively (default *p*-value cutoff 1e-5). Given the genomic positions of peak summits and gene structure information (“refGene.txt” from UCSC Genome Browser database), we annotated each peak summit with the corresponding genomic structure using our custom script and count the number of peak summits for each gene structure [5]. For RNA-Seq, we obtained 85,770,572 and 82,896,315 uniquely-mapped reads for ST*Hdh*Q7/7 and ST*Hdh*Q111/111 respectively. Then, we estimated and normalized gene expression levels by RPKM (reads per kilobase per million mapped reads) using the reads and the 27,346 mouse RefSeq genes [15].

Next, in order to identify transcriptome landscaped by H3K9me3 (that are highly occupied by H3K9me3 in their promoter regions and, in parallel, their RNA expressions are down regulated), we further analyzed data from H3K9me3 ChIP-seq and RNA-seq by platform integration analysis (Fig. 2b, Supplementary Table 1 and 2). Down-regulated genes putatively influenced by high H3K9me3 occupancy are marked in red and the up-regulated genes with low H3K9 occupancy are marked in blue. Green dotted lines indicate the fold cutoff (log2ratio 1 or −1). The level of H3K9me3 occupancy was found to be specifically increased in two regions, the 5′-UTR and within the 5′ edge of the CDS (Fig. 2c). The chromosomal occupancy of H3K9me3 is shown in Supplementary Figure 3. Furthermore, we performed functional enrichment analysis and found that 56 genes among the 545 genes are mainly involved in processes associated with synaptic transmission (synaptic transmission and axon guidance), calcium signaling, regulation of the actin cytoskeleton (cell migration, focal adhesion, and the integrin-mediated signaling pathway; Supplementary

Table 1). We then generated a biological network to delineate relationships among the 56 genes and their associated processes as shown in Fig. 2d. The network shows dense connections between the nodes associated with the processes in the network, indicating that H3K9me3 collectively regulates synaptic transmission and actin cytoskeleton related processes.

Verification of H3K9me3-landscaped transcriptome

To determine whether alterations of the transcriptome landscaped by H3K9me3 are apparent in HD, we assessed the occupancy of H3K9me3 and mRNA levels of target genes in mouse and human HD samples as well as in an HD cell line (Fig. 3 and Fig. S4). Fig. 3a displays ChIP and qPCR results with primers specific to the CHRM1, PDGFB, and INPP5J genes. H3K9me3 occupancy was increased within the promoters of CHRM1, PDGFB, and INPP5J while mRNAs of CHRM1, PDGFB, and INPP5J were decreased in HD Q111 cells. Other genes such as Hrh1, IRF6, EYA1, and KIF5C also exhibited increased occupancy of H3K9me3 and reduced mRNA levels (Fig. S4). Next, we performed Western blot and densitometry analysis to verify the protein level of H3K9me3-target genomes in HD striatal cells, transgenic HD (R6/2) mice and human HD patients. As expected, the protein level of CHRM1 was markedly decreased in ST*Hdh*Q7/7 cells compared to ST*Hdh*Q111/111 cells (Fig. 4a). CHRM1 immunoreactivity and mRNA were significantly decreased in striatal neurons of HD (R6/2 line) mice (Fig. 4b, c). Consistent with data from mouse and the cellular model of HD, ChRM1 immunoreactivity was significantly reduced in the caudate and putamen of HD brains (Fig. 4d). CHRM1 mRNA was decreased by 40% ($p< 0.05$) in striatal tissue samples compared to controls (Fig. 4e). Moreover, CHRM1 protein levels were also significantly reduced in the striatum of transgenic HD (R6/2) mice and HD human brain compared to controls respectively (Fig. 4f, g).

Cholinergic muscarinic receptors are classified into M1–M5 receptors. The receptors are distinguished by location, post-receptor signaling pathway and agonist or antagonist interaction. The CHRM1 is the most significant muscarinic receptor in the CNS and is highly expressed in neurons. We determined the relative levels of other CHRM isoforms. Interestingly, neither CHRM2 nor 4 levels were significantly altered in an HD cell line or in HD mice (Fig. S5). Our study confirms that CHRM1 is specifically modulated by heterochromatin condensation while CHRM2 isoform is not reduced in HD cells or in HD mice. Otherwise, CHRM3 levels were significantly reduced in the HD cell line, transgenic HD mice and human HD patients (Fig. S5).

To verify whether the plasticity of heterochromatin condensation drives the expression of the CHRM1 gene, we established a Tet-inducible ESET, a histone H3K9-specific trimethyltransferase, cell line (Fig. 5a, see Supplementary Methods). As we expected, the expression of CHRM1 was down regulated when ESET was induced by doxycycline (Doxy) and H3K9me3 levels were increased. In contrast, halting ESET induction restored the expression of CHRM1 by reducing H3K9me3 levels (Fig. 5b). These data show that CHRM1 gene expression is modulated by H3K9me3-dependent heterochromatin plasticity. In addition, surprisingly, CHRM3 expression was down regulated when ESET and H3K9me3 were induced by doxycycline (Doxy) (Fig. S6). Further studies to determine how CHRM3 gene transcription is regulated will be needed to better understand the molecular basis and regional specificity of CHRM-mediated cholinergic activation in the brain.

Deregulation of CHRM1 expression impairs Ca^{2+} response in striatal cells

The CHRM-mediated Gq-PLC beta pathway is a major signaling transduction pathway produced by muscarinic receptor activation. Once the activated PLC beta hydrolyzes PIP2 into IP3 and DAG, IP3 increases intracellular calcium from Ca^{2+} stores such as the ER via

the IP3 receptor. Since CHRM1 mRNA and protein are reduced in striatal neurons of HD and CHRM1 regulates Ca^{2+} release through endoplasmic reticulum (ER), we examined whether CHRM1-dependent signaling pathways are impaired and whether intracellular Ca^{2+} is altered in HD striatal (ST*Hdh*Q111/111 and ST*Hdh*Q7/7) cells. We measured changes in intracellular Ca2+ in response to Ach stimulation using Fura 2-AM in STHdhQ7/7 and STHdhQ111/111 cells (Fig 6a). We found that Ach stimulation increases intracellular Ca^{2+} as determined by ratio of fluorescence absorbance at 340/380 (Fig 6a). Using the data shown in Figure 5a, we analyzed 1) the basal level of Ca^{2+} before the application of Ach, 2) the peak Ca^{2+} response to Ach, and 3) Δchange of intracellular Ca^{2+} level induced by Ach. Interestingly, basal intracellular Ca^{2+} levels were higher in ST*Hdh*Q111/111 cells than in ST*Hdh*Q7/7 cells, indicating that the Ca^{2+} buffering system is altered in the ST*Hdh*Q111/111 cells (Fig. 6b) [20, 21]. As expected, Δchange of intracellular Ca^{2+} level was significantly lower in ST*Hdh*Q111/111 than in ST*Hdh*Q7/7 cells after Ach treatment (Fig. 6c). Thapsigargin (TG), an intracellular Ca^{2+} immobilizer, blocked the peak induction of intracellular Ca^{2+} response by Ach, indicating that Ca^{2+} stored in ER mediates Ach signaling in striatal cells (Fig. S7). In addition, we confirmed that pirenzepine, a CHRM1 specific antagonist, abrogated the Ach-induced intracellular Ca^{2+} response (Fig. 6d) while methoctramine, a CHRM2 inhibitor, did not block the Ach-induced intracellular Ca^{2+} response (Fig. 6e). Our results show that CHRM1 is a functional muscarinic receptor that induces intracellular Ca2+ signaling in response to Ach in striatal cells and that deregulation of ChRM1 gene expression resulting from structural changes in heterochromatin condensation leads to impaired Ca2+ release from ER.

Discussion

Medium spiny neurons (MSNs) are major projection neurons in the striatum and serve as the main synaptic target of cholinergic interneurons [2]. While MSNs are GABAergic neurons, constituting more than 95% of striatal cell population, cholinergic interneurons are relatively large (20–50 mm) aspiny neurons that account for only 1–2% of the total neuronal population of the striatum. Cholinergic interneurons relay inputs from dopaminergic fibers to the MSNs and Ach from interneurons modulates striatal synaptic transmission via cholinergic receptors, which produces both short-term and long-term effects [2]. Ach-mediated neurotransmission has a crucial role in the control of voluntary movement exerted by the striatum and, accordingly, this brain area contains some of the highest levels of Ach, muscarinic receptors and other Ach-related markers in the CNS. Muscarinic Ach receptor family consists of five subtypes, CHRM1-CHRM5 with high homologous protein sequences [1]. However, they exhibit differences in signal transduction mediated via G protein-coupled pathways and result in different physiological responses [10, 28]. While CHRM1, CHRM3, and CHRM5 show selectivity for G proteins of the Gq/11 family, CHRM2 and CHRM4 preferentially couple to Gi/o-type G proteins. CHRM1 promotes phosphatidylinositol (PtdIns) hydrolysis and intracellular Ca^{2+} mobilization, whereas CHRM2 is coupled negatively to adenylate-cyclase activity [10]. Thus, a heterogeneous population of muscarinic receptors are involved in the mediating cholinergic action on glutamatergic and GABAergic nerve terminals in the stiratum [23]. Importantly, the striatal cholinergic system has been implicated in the pathophysiology of HD, but the cellular mechanisms underlying the epigenetic regulation of CHRM expression in striatal neurons are not known.

Epigenetic histone modifications promote alterations in chromatin packaging that result in transcriptional repression in HD. The increase of H3K9me3 level has been correlated with the formation of large constitutive heterochromatin domains and is thought to promote gene silencing in both local and global repression of transcription [12, 30]. We have found that altered expression of histone methyltransferase (HMT) and elevated H3K9me3 are linked to upstream transcriptional deregulation in both animal models of HD and in HD patients [6,

18, 22]. Our current data further establishes a novel epigenetic pathway whereby H3K9me3-dependent heterochromatin condensation leads to transcriptional deregulation of CHRM1 by occupying its promoter in HD striatal cells. Since Ach plays a key role in the regulation of striatal output by influencing the activity of GABAergic medium spiny neurons, the interaction of Ach with pre- and postsynaptic CHRMs is pivotal to modulate the striatal activity. Accordingly, the net effect of GABAergic MSNs is dependent upon the expression type and location of the muscarinic receptors [27, 29]. The conventional wisdom is that loss of cholinergic receptor function directly results in synaptic dysfunction through inadequate intracellular signal transductions in neurons. The CHRM is highly expressed in the striatum of control brain but is down regulated in HD striatum [2, 3]. In this context, our findings that increased occupancy of H3K9me3 in the promoter of CHRM1 and decreased level of CHRM1 mRNA provide a molecular epigenetic mechanism that may explain how CHRM1 is regulated at the transcriptional level and why function is altered in HD. Our pharmacological data further confirms that CHRM1 is a major muscarinic receptor transducing intracellular Ca^{2+} signaling. Reduced CHRM1 protein levels result in the deregulation of intracellular Ca^{2+} release from ER in response to Ach in HD striatal cells (Fig. 7). Because CHRM3 is known to show a selectivity for G protein-coupled signal transduction similar to that found in CHRM1-mediated pathways, the down regulation of CHRM3 expression could also contribute to the deregulation of intracellular Ca^{2+} mobilization in HD [13, 14]. Future studies on both CHRM3 and CHRM1 in striatal cells will be needed to better understand Ach-dependent synaptic activity in the striatum where Ach receptors heterogeneity exists.”

In summary, our data show that epigenetic regulation of CHRM1 and genomes landscaped by H3K9me3 are relevant to the pathogenesis of HD. H3K9me3-dependent heterochromatin condensation leads to transcriptional repression of CHRM1 and deregulation of Ach-induced intracellular Ca^{2+} signaling. Changes in H3K9me3 and CHRM1 levels may prove to be useful indicators of HD onset and progression. Since CHRM1 receptor agonists have been receiving more attention as potential treatments for neurodegenerative diseases [16], CHRM1 agonists could help ameliorate some of the symptoms of HD and other movement disorders.

Supplementary Material

Refer to Web version on PubMed Central for supplementary material.

Acknowledgments

We thank to Dr. Marcy MacDonald for ST*HdhQ7/7* and ST*HdhQ111/111* cells and to Min-Kyung Jung for her technical assistance. This study was supported by WCU Neurocytomics Program Grant (800-20080848) (H.R.) and SRC Grant (2010-0029-403) (H.R.) from MEST of Korea, Flagship Grant (H.R.) from KIST and NIH NS 067283-01A1 (H.R.).

References

1. Bonner TI, Buckley NJ, Young AC, Brann MR. Identification of a family of muscarinic acetylcholine receptor genes. Science. 1987; 237:527–532. [PubMed: 3037705]
2. Calabresi P, Centonze D, Gubellini P, Pisani A, Bernardi G. Acetylcholine-mediated modulation of striatal function. Trends Neurosci. 2000; 23:120–126. [PubMed: 10675916]
3. Cha JH, Kosinski CM, Kerner JA, Alsdorf SA, Mangiarini L, Davies SW, Penney JB, Bates GP, Young AB. Altered brain neurotransmitter receptors in transgenic mice expressing a portion of an abnormal human Huntington disease gene. Proc Natl Acad Sci USA. 1998; 95:6480–6485. [PubMed: 9600992]

4. Ekins S, Nikolsky Y, Bugrim A, Kirillov E, Nikolskaya T. Pathway mapping tools for analysis of high content data. Methods Mol Biol. 2007; 356:319–350. [PubMed: 16988414]
5. Fujita PA, Rhead B, Zweig AS, Hinrichs AS, Karolchik D, Cline MS, Goldman M, Barber GP, Clawson H, Coelho A, Diekhans M, Drezer TR, Giardine BM, Harte RA, Hillman-Jackson J, Hsu F, Kirkup V, Kuhn RM, Learmed K, Li CH, Meyer LR, Pohl A, Raney BJ, Rosenbloom KR, Smith KE, Haussler D, Kent WJ. The UCSC Genome Browser database: update 2011. Nucleic Acids Res. 2011; 39:D876–882. [PubMed: 20959295]
6. Gardian G, Browne SE, Choi DK, Klivenyi P, Gregorio J, Kubilus JK, Ryu H, Langley B, Ratan RR, Ferrante RJ, Beal MF. Neuroprotective effects of phenylbutyrate in the N171-82Q transgenic mouse model of Huntington's disease. J Biol Chem. 2005; 280:556–563. [PubMed: 15494404]
7. Grewal SI, Jia S. Heterochromatin revisited. Nat Rev Genet. 2007; 8:35–46. [PubMed: 17173056]
8. Hake SB, Xiao A, Allis CD. Linking the epigenetic language of covalent histone modifications to cancer. Br J Cancer. 2004; 90:761–769. [PubMed: 14970850]
9. Huang da W, Sherman BT, Lempicki RA. Systematic and integrative analysis of large gene lists using DAVID bioinformatics resources. Nat Protoc. 2009; 4:44–57. [PubMed: 19131956]
10. Hulme EC, Birdsall NJM, Buckley NJ. Muscarinic receptor subtypes. Ann Rev Pharmacol and Toxicol. 1990; 30:633–673. [PubMed: 2188581]
11. Junker BH, Koschutzki D, Schreiber F. Exploration of biological network centralities with CentiBiN. BMC Bioinformatics. 2006; 7:219. [PubMed: 16630347]
12. Lee J, Hagerty S, Cormier KA, Kung AL, Ferrante RJ, Ryu H. Monoallele deletion of CBP leads to pericentromeric heterochromatin condensation through ESET expression and histone H3 (K9) methylation. Hum Mol Genet. 2008; 17:1774–1782. [PubMed: 18319327]
13. Lim D, Fedrizzi L, Tartari M, Zuccato C, Cattaneo E, Brini M, Carafoli E. Calcium homeostasis and mitochondrial dysfunction in striatal neurons of Huntington disease. J Biol Chem. 2008; 283:5780–5789. [PubMed: 18156184]
14. Milakovic T, Quintanilla RA, Johnson GV. Mutant huntingtin expression induces mitochondrial calcium handling defects in clonal striatal cells: functional consequences. J Biol Chem. 2006; 281:34785–34795. [PubMed: 16973623]
15. Mortazavi A, Williams BA. Mapping and quantifying mammalian transcriptomes by RNA-Seq. Nat Methods. 2008; 5:621–628. [PubMed: 18516045]
16. Pisani A, Bernardi G, Ding J, Surmeier DJ. Re-emergence of striatal cholinergic interneurons in movement disorders. Trends Neurosci. 2007; 30:545–553. [PubMed: 17904652]
17. Ryu H, Lee J, Impey S, Ratan RR, Ferrante RJ. Antioxidants Modulate Mitochondrial Protein Kinase A and Increase CREB Binding to D-Loop DNA of the Mitochondrial Genome in Neurons. Proc Natl Acad Sci USA. 2005; 102:13915–13920. [PubMed: 16169904]
18. Ryu H, Lee J, Hagerty SW, Soh BY, McAlpin SE, Cormier KA, Smith KM, Ferrante RJ. ESET/SETDB1 gene expression and histone H3 (K9) trimethylation in Huntington's disease. Proc Natl Acad Sci USA. 2006; 103:19176–19181. [PubMed: 17142323]
19. Sadri-Vakili G, Cha JH. Mechanisms of disease: Histone modifications in Huntington's disease. Nat Clin Pract Neurol. 2006; 2:330–338. [PubMed: 16932577]
20. Schultz DC, Ayyanathan K, Negorev D, Maul GG, Rauscher FJ 3rd. SETDB1: a novel KAP-1-associated histone H3, lysine 9-specific methyltransferase that contributes to HP1-mediated silencing of euchromatic genes by KRAB zinc-finger proteins. Genes Dev. 2002; 16:919–932. [PubMed: 11959841]
21. Shannon P, Markiel A, Qzier O, Baliga NS, Wang JT, Ramage D, Amin N, Schwikowski B, Ideker T. Cytoscape: a software environment for integrated models of biomolecular interaction networks. Genome Res. 2003; 13:2498–2504. [PubMed: 14597658]
22. Stack EC, Del Signore SJ, Luthi-Carter R, Soh BY, Goldstein DR, Matson S, Goodrich S, Markey AL, Cormier K, Hagerty SW, Smith K, Ryu H, Ferrante RJ. Modulation of nucleosome dynamics in Huntington's disease. Hum Mol Genet. 2007; 16:1164–1175. [PubMed: 17403718]
23. Sugita S, Uchimura N, Jiang ZG, North RA. Distinct muscarinic receptors inhibit release of GABA and excitatory amino acids in mammalian brain. Proc Natl Acad Sci USA. 1991; 88:2608–2611. [PubMed: 1672454]

24. The Huntington's Disease Collaborative Research Group. A novel gene containing a trinucleotide repeat that is expanded and unstable on Huntington's disease chromosomes. Cell. 1993; 72:971–983. [PubMed: 8458085]
25. Trettel F, Rigamonti D, Hilditch-Maguire P, Wheeler VC, Sharp AH, Persichetti F, Cattaneo E, MacDonald ME. Dominant phenotypes produced by the HD mutation in STHdh (Q111) striatal cell. Hum Mol Genet. 2000; 9:2799–2809. [PubMed: 11092756]
26. Wang H, An W, Cao R, Xia L, Erdjument-Bromage H, Chatton B, Tempst P, Roeder RG, Zhang Y. mAM facilitates conversion by ESET of dimethyl to trimethyl lysine 9 of histone H3 to cause transcriptional repression. Mol Cell. 2003; 12:475–487. [PubMed: 14536086]
27. Wang Z, Kai L, Day M, Ronesi J, Yin HH, Ding J, Tkatch T, Locinger DM, Surmeier DJ. Dopaminergic control of corticostriatal long-term synaptic depression in medium spiny neurons is mediated by cholinergic interneurons. Neuron. 2006; 50:443–452. [PubMed: 16675398]
28. Wess J. Molecular biology of muscarinic acetylcholine receptors. Crit Rev Neurobiol. 1996; 10:69–99. [PubMed: 8853955]
29. Wilson CJ. Striatal D2 receptors and LTD: yes, but not where you thought they were. Neuron. 2006; 50:347–348. [PubMed: 16675388]
30. Wu R, Terry AV, Singh PB, Gilbert DM. Differential subnuclear localization and replication timing of histone H3 lysine 9 methylation states. Mol Biol Cell. 2005; 16:2872–2881. [PubMed: 15788566]
31. Wu R, Singh PB, Gilbert DM. Uncoupling global and fine-tuning replication timining determinants for mouse pericentric heterochromatin. J Cell Biol. 2006; 174:185–194. [PubMed: 16831888]
32. Wu TD, Nacu S. Fast and SNP-tolerant detection of complex variants and splicing in short reads. Bioinformatics. 2010; 26:873–881. [PubMed: 20147302]
33. Yamada M, Sato T, Shimohata T, Hayashi S, Igarashi S, Tsuji S, Takahashi H. Interaction between neuronal intranuclear inclusions and promyelocytic leukemia protein nuclear and coiled bodies in CAG repeat diseases. Am J Pathol. 2001; 159:1785–1795. [PubMed: 11696439]
34. Yang L, Xia L, Wu DY, Wang H, Chansky HA, Schubach WH, Hickstein DD, Zhang Y. Molecular cloning of ESET, a novel histone H3-specific methyltransferase that interacts with ERG transcription factor. Oncogene. 2002; 21:148–152. [PubMed: 11791185]
35. Zhang Y, Reinberg D. Transcription regulation by histone methylation: interplay between different covalent modifications of the core histone tails. Genes Dev. 2001; 15:2343–2360. [PubMed: 11562345]
36. Zhang Y, Liu T, Meyer CA. Eeckhoute J, Johnson DS, Bernstein BE et al. Model-based Analysis of ChIP-Seq (MACS). Genome Biol. 2008; 9:R137. [PubMed: 18798982]

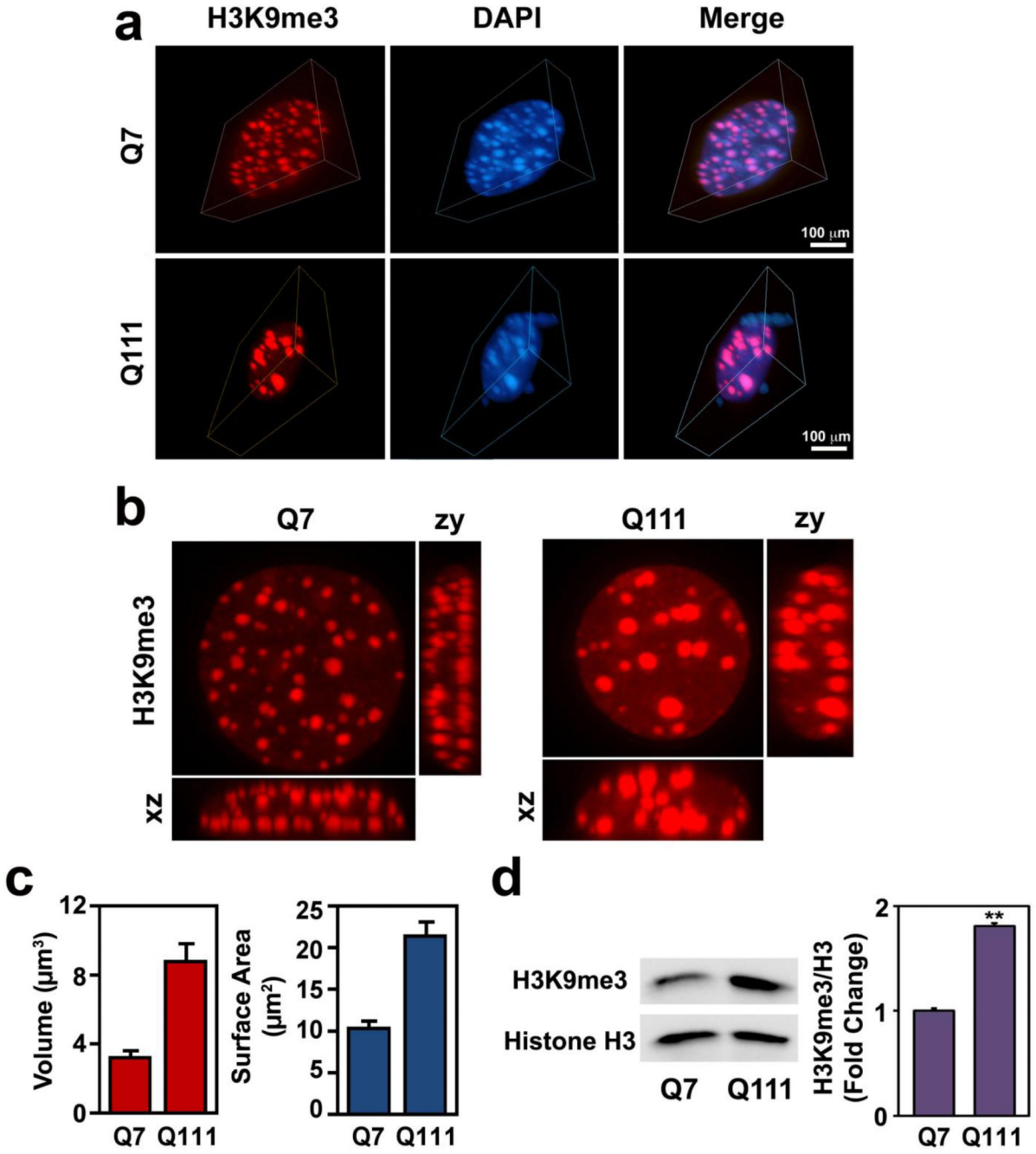

Fig. 1.

The trimethylated histone H3K9 (H3K9me3)-dependent pericentromeric heterochromatin is condensed in HD cells. **a** 3-D reconstruction images show intense staining of H3K9me3 (red) and pericentromeric heterochromatin condensation (blue) in mutant huntingtin (mtHtt) striatal cells (ST*Hdh*Q111/Q111) compared to control (ST*Hdh*Q7/Q7) cells. **b** Analysis of xz and zy stacked images showed the dynamic difference of spatial H3K9me3 distribution between ST*Hdh*Q7/Q7 and ST*Hdh*Q111/Q111 cells. **c** Volumetric expansion of H3K9me3-dependent pericentromeric heterochromatin is found in ST*Hdh*Q111/Q111 cells. **d**. Western

blot analysis showed a significant increase in H3K9me3 levels in ST*Hdh*Q111/Q111 cells compared to ST*Hdh*Q7/7 (Q7) cells. [$p<0.05$ (*)]."

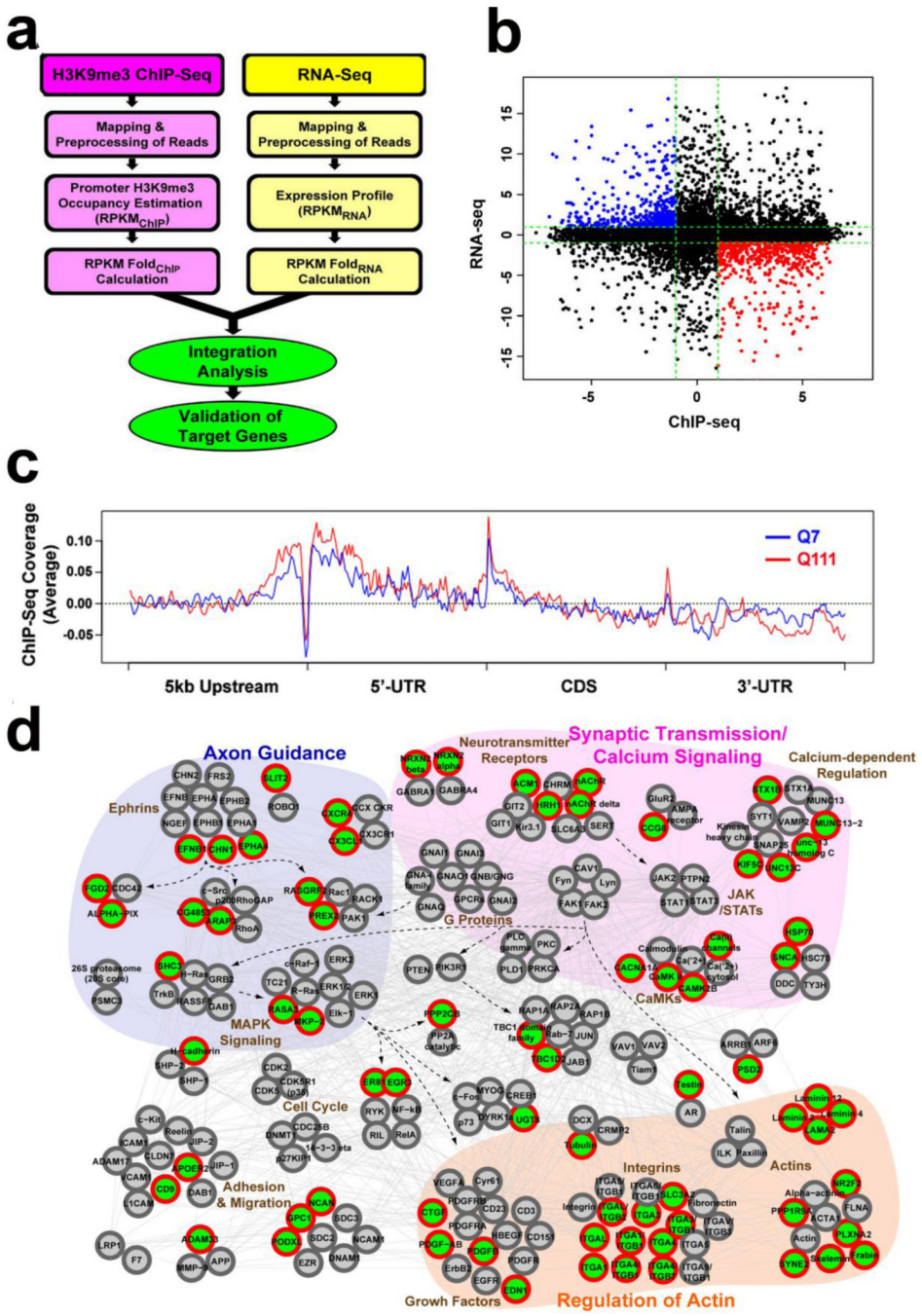

Fig. 2.

H3K9me3-landscaped transcriptome is analyzed by integrating data from H3K9me3 ChIP-sequencing and RNA-sequencing in HD cells. **a** A scheme representing the integration strategy used to identify H3K9me3-landscaped and heterochromatin-associated transcriptome in ST*Hdh*Q7/Q7 and ST*Hdh*Q111/Q111 cells. **b** Integration of data from H3K9me3 ChIP-seq and RNA-seq. Down-regulated genes putatively influenced by high H3K9me3 occupancy are marked in red and the up-regulated genes with low H3K9 occupancy are marked in blue. Green dotted lines indicate the fold cutoff (log2ratio 1 or −1). **c** Gene structural occupancy by H3K9me3. The H3K9me3 occupancies for 4 different gene structures (5kb upstream, 5′ UTR, CDS, and 3′ UTR) were calculated. **d** A hypothetical

network delineating major neuronal processes represented by the 545 genes involved in synaptic transmission/calcium signaling, axon guidance, and actin cytoskeleton-related processes. Node and boundary colors denote the decrease (green) of mRNA expression levels and the increase (red) of H3K9me3, respectively. Gray color represents no change in mRNA expression levels or H3K9me3. The arrows represent activation information obtained from KEGG pathways.

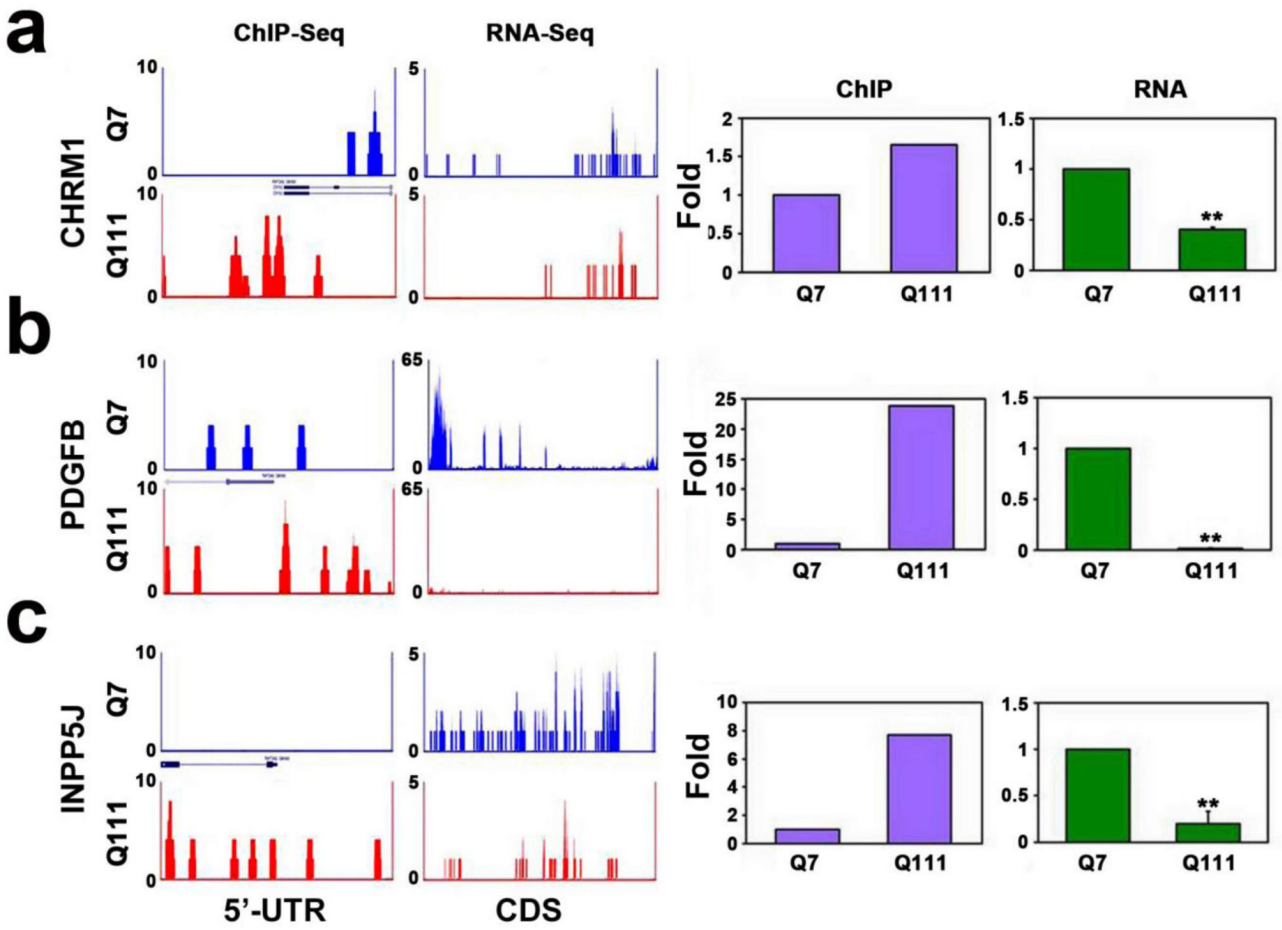

Fig. 3.

Verification of H3K9me3-landscaped transcriptome by quantitative real-time PCR. **a** Cholinergic receptor muscarinic type 1 (CHRM1), a synaptic transmission gene, is down regulated in ST*Hdh*Q111/Q111 cells. **b** INPP5J, an inositol phosphate signaling molecule, is down regulated in ST*Hdh*Q111/Q111 cells. **c** PDGFB, a neuronal growth factor, is down regulated in ST*Hdh*Q111/Q111 cells.

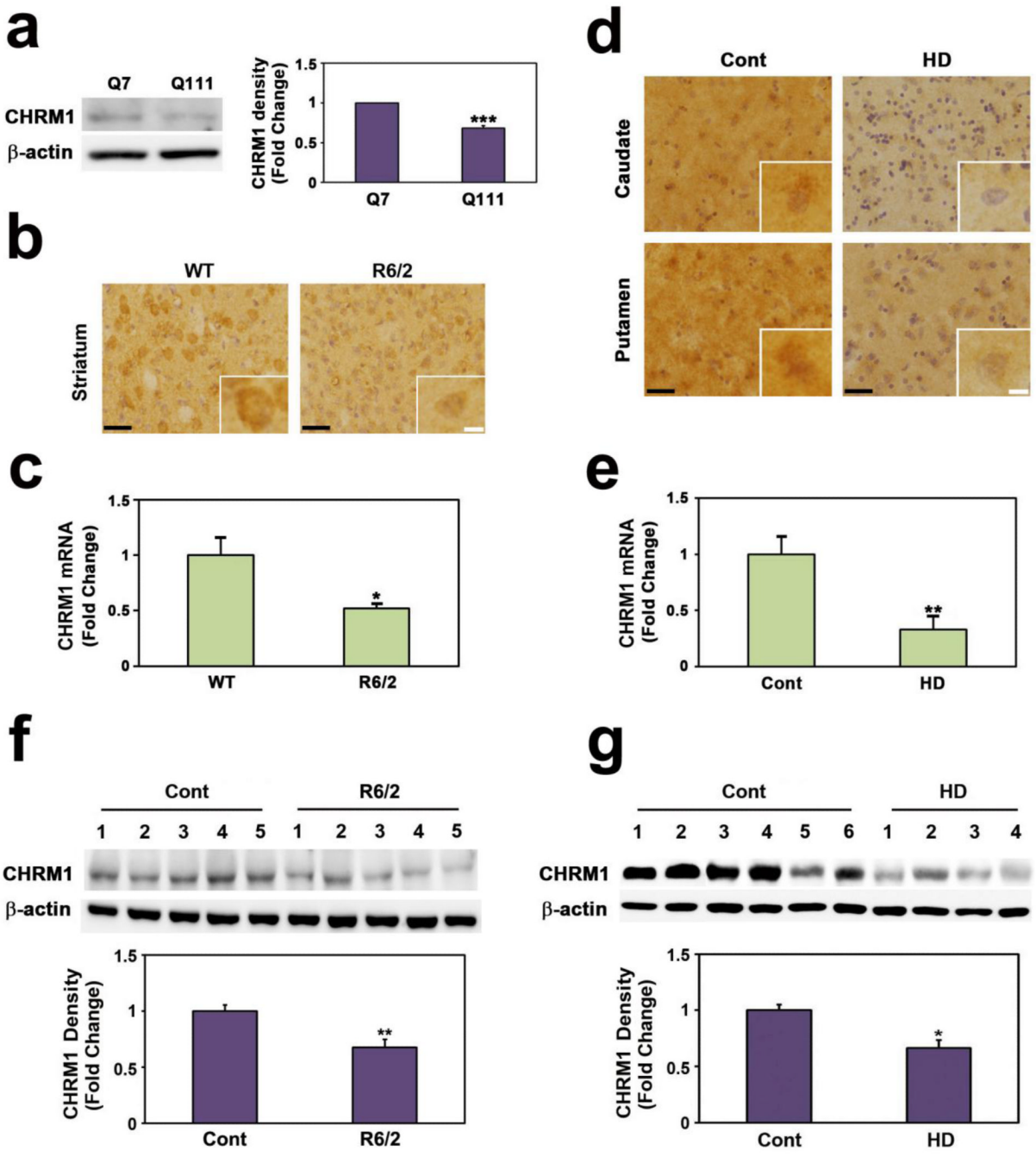

Fig. 4.

CHRM1 gene is down regulated in HD. **a** Western blot data and densitometry analysis showed a marked decrease of CHRM1 protein levels in ST*Hdh*Q111/Q111 cells in comparison to ST*Hdh*Q7/7 cells. **b** CHRM1 immunoreactivity is markedly decreased in the striatum of R6/2 HD mice. Scale bar: black, 30μm; white, 5μm. Magnification, 40×. **c** CHRM1 mRNA is down regulated in the striatal neurons of R6/2 HD mice. **d** CHRM1 immunoreactivity is decreased in the caudate and putamen of human HD patients. Scale bar: black, 30μm; white, 5μm. Magnification, 40×. **e** The level of CHRM1 mRNA is down regulated in striatum of human HD patients. **f**. The protein levels CHRM1 were markedly

reduced in HD (R6/2) mice. **g** CHRM1 protein levels were decreased in human HD patients. The level of CHRM1 was normalized to β-actin. Significantly different at $p<0.05$ (*) and $p<0.005$ (**).”

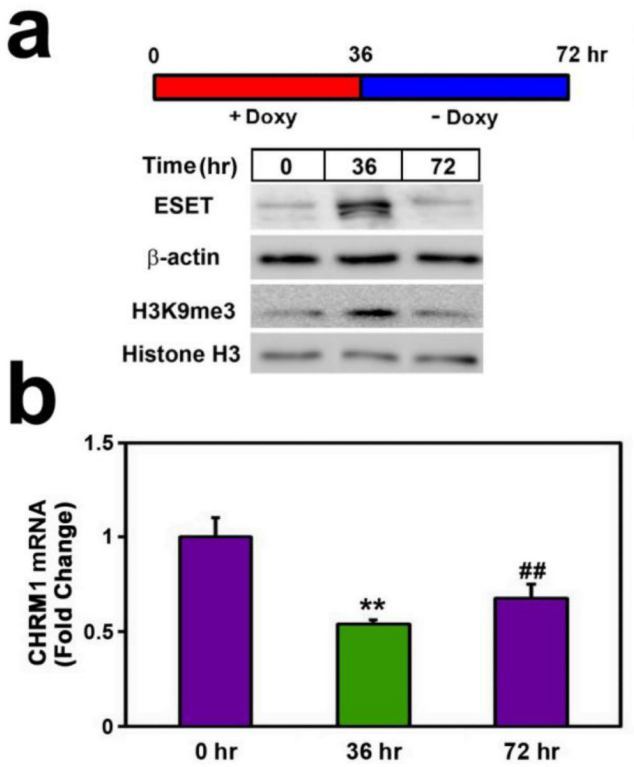

Fig. 5.

The expression of CHRM1 mRNA is regulated by the plasticity of H3K9me3-dependent heterochromatin driven by ESET expression. **a** A schematic representation of Tet-inducible ESET cell line system. Cells were treated with doxycycline (+Doxy) for 36hr to turn on ESET expression. Cells were then washed out doxycycline (−Doxy) and switched to the normal media for another 36hr to turn off ESET expression. The Doxy-induced cells showed an increase of H3K9me3 along with ESET. In Doxy-off cells, the level of H3K9me3 was decreased along with ESET. **b** The induction of ESET and H3K9me3 by Doxy down regulated the expression of CHRM1. Data are mean ± SE of three separate experiments. **, Significantly different from 0 hr at $p<0.01$; ##, significantly different from 36hr at $p<0.01$.

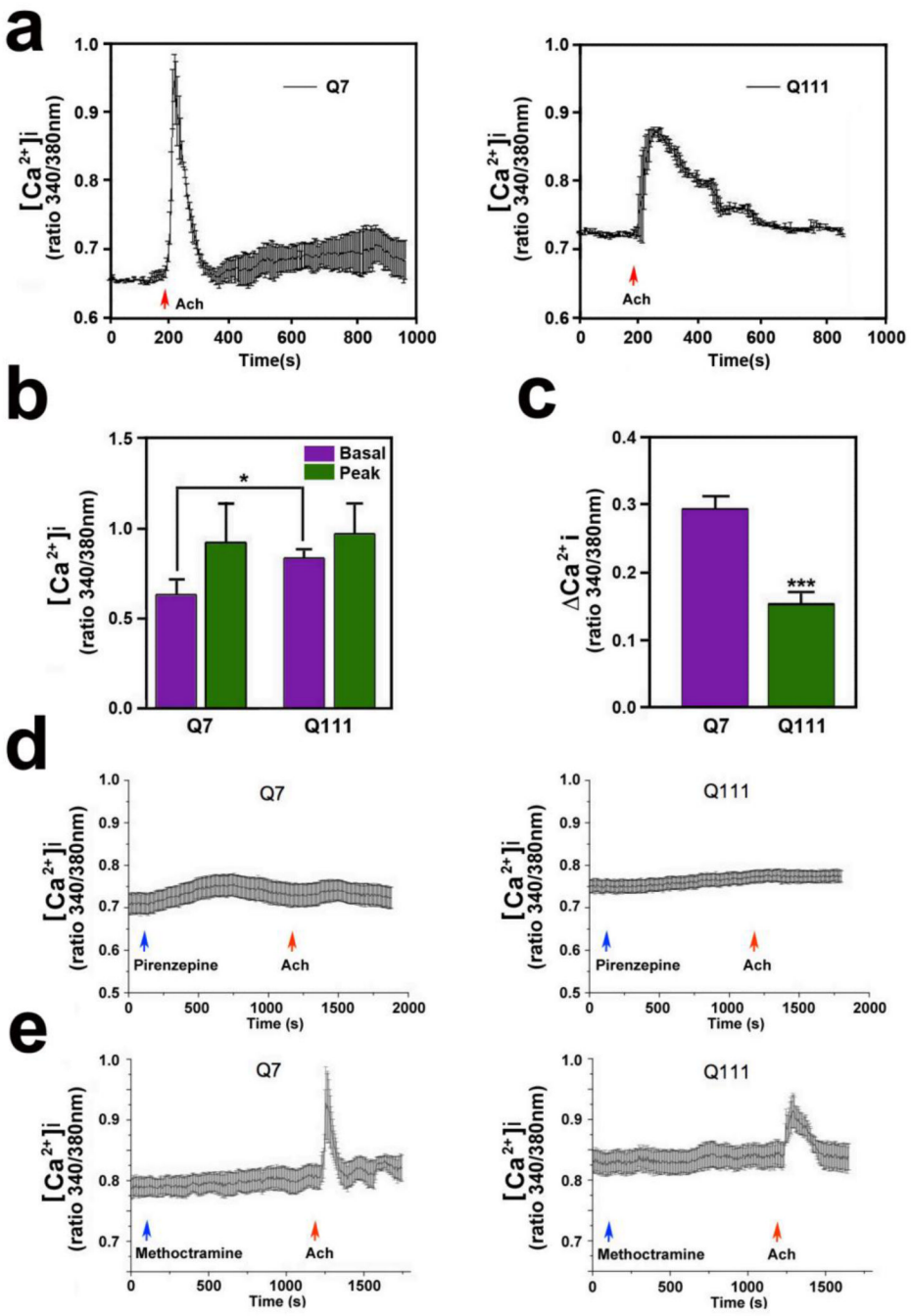

Fig. 6.

Intracellular Ca^{2+} response to acetylcholine (Ach) is impaired in HD cells. **a** Intracellular Ca^{2+} ($[Ca^{2+}]i$) response to Ach stimulation is different between ST*Hdh*Q7/7 and ST*Hdh*Q111/111 cells. **b** The basal and peak levels of intracellular Ca^{2+} are altered in ST*Hdh*Q111/111 cells compared to ST*Hdh*Q7/7 cells. **c** Changes of intracellular Ca^{2+} ($DCa^{2+}i$) levels are altered in ST*Hdh*Q111/111 cells. **d** The CHRM1 specific antagonist pirenzepine abrogated the Ach-induced intracellular Ca^{2+} response. **e** The CHRM2 inhibitor, methoctramine, does not block the Ach-induced intracellular Ca^{2+} response.

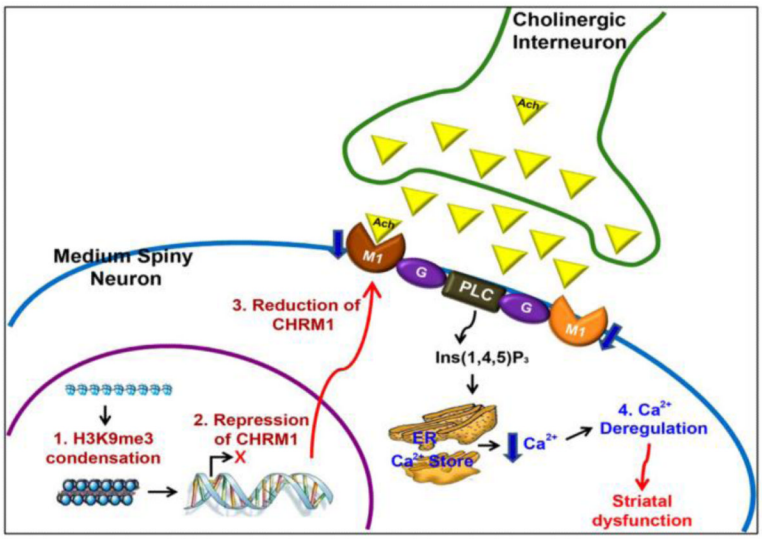

Fig. 7.

A scheme illustrates how epigenome contributes to neurodegeneration. CHRM1-dependent striatal synaptic function is impaired in HD. H3K9me3-induced heterochromatin condensation leads to the repression of *CHRM1* gene and subsequent reduction of CHRM1 protein in medium spiny neurons (1-3). Down regulation of CHRM1 leads to alterations of acetylcholine (Ach) response and intracellular Ca^{2+} dynamics, which affects on the synaptic function of striatum (4).